Comparison of AVIRIS and Hyperion for Hyperspectral Mineral Mapping[**]

Fred A. Kruse[1]

1.0 Introduction

The 0.4 to 2.5 µm spectral range provides abundant information about many important Earth-surface minerals (Clark et al., 1990). In particular, the 2.0 to 2.5 µm spectral range covers spectral features of hydroxyl-bearing minerals, sulfates, and carbonates common to many geologic units and hydrothermal alteration assemblages. Imaging Spectrometers, or "Hyperspectral" sensors provide the unique combination of both spatially contiguous spectra and spectrally contiguous images of the Earth's surface that allows spatial mapping of these minerals (Goetz et al., 1985). Airborne hyperspectral data have been available to researchers since the early 1980s and their use for mineral mapping is well established (Goetz et al., 1985; Kruse and Lefkoff, 1993; Boardman and Kruse, 1994; Boardman et al., 1995; Kruse, et al., 1999). Current airborne sensors provide high-spatial resolution (2-20m), high-spectral resolution (10-20nm), and high SNR (>500:1) data for a variety of scientific disciplines (Green et al., 2001; Kruse et al., 2000).

NASA's EO-1 Hyperion sensor, launched in November 2000, is a test bed instrument designed to demonstrate hyperspectral imaging from space (Pearlman et al., 1999). Science validation efforts are in progress and selected AIG/CSIRO Hyperion results demonstrating mineral mapping have previously been presented and published (Kruse et al., 2001, 2002). New details and accuracy assessment compared to AVIRIS data are presented here.

2.0 Comparison of AVIRIS And Hyperion Specifications

The Airborne Visible/Infrared Imaging Spectrometer (AVIRIS) represents the current state of the art airborne hyperspectral system (Porter and Enmark, 1987; Green et al., 2001). AVIRIS, flown by NASA/Jet Propulsion Laboratory (JPL) is a 224-channel imaging spectrometer with approximately 10 nm spectral resolution covering the 0.4 – 2.5 µm spectral range. The sensor is a whiskbroom system utilizing scanning foreoptics to acquire cross-track data. The IFOV is 1 milliradian. Four off-axis double-pass Schmidt spectrometers receive incoming illumination from the foreoptics using optical fibers. Four linear arrays, one for each spectrometer, provide high sensitivity in the 0.4 to 0.7 µm, 0.7 to 1.2 µm, 1.2 to 1.8 µm, and 1.8 to 2.5 µm regions respectively. AVIRIS is flown as a research instrument on the NASA ER-2 aircraft at an altitude of approximately 20 km, resulting in approximately 20-m pixels and a 10.5-km swath width. Since 1998, it has also been flown on a Twin Otter aircraft at low altitude, yielding 2 – 4m spatial resolution.

The launch of NASA's EO-1 Hyperion sensor in November 2000 marked the establishment of spaceborne hyperspectral mineral mapping capabilities. Hyperion is a satellite hyperspectral sensor covering the 0.4 to 2.5 µm spectral range with 242 spectral bands at approximately 10nm spectral resolution and 30m spatial resolution from a 705km orbit (Pearlman et al., 1999). Hyperion is a pushbroom instrument, capturing 256 spectra over a 7.5Km-wide swath perpendicular to the satellite motion. The system has two grating spectrometers; one visible/near infrared (VNIR) spectrometer (approximately 0.4 – 1.0 µm) and one short-wave infrared (SWIR) spectrometer (approximately 0.9 – 2.5 µm). Data are calibrated to radiance using both pre-mission and on-orbit measurements. Table 1 shows a comparison of key AVIRIS and Hyperion characteristics.

Table 1: AVIRIS/Hyperion Sensor Characteristics Comparison

HSI Sensor	Spectral Resolution	Spatial Resolution	Swath Width	SWIR SNR
AVIRIS-High Altitude	10 nm	20 m	12 km	~500:1
Hyperion	10 nm	30 m	7.5 km	~50:1

[**] Presented at the 11th JPL Airborne Geoscience Workshop, 4-8 March 2002, Pasadena, California
[1] Analytical Imaging and Geophysics LLC, Boulder, Colorado, USA, E-mail: kruse@aigllc.com

3.0 Basic Hyperspectral Mineral mapping – Cuprite, Nevada

3.1 Site Description

Cuprite, Nevada, located approximately 200 km northwest of Las Vegas (Figure 1) is a relatively undisturbed acid-sulfate hydrothermal system exhibiting well exposed alteration mineralogy consisting principally of kaolinite, alunite, and hydrothermal silica. The geology and alteration were previously mapped in detail (Abrams et al., 1977; Ashley and Abrams, 1980). Swayze (1997) includes a good geologic summary, a generalized geologic map, and detailed mineral maps derived from 1990 and 1994 AVIRIS data. Cuprite, has been used as a geologic remote sensing test site since the early 1980s and many studies have been published (Goetz et al., 1985; Ashley and Abrams, 1980; Goetz. and Strivastava,, 1985; Swayze., 1997; Shipman and Adams, 1987; Kruse et al., 1990; Hook, 1990; Swayze et al., 1992; Goetz and Kindel, 1996; Kruse et al, 2002)

Figure 1: Cuprite, Nevada, Location map.

This study compares mineral mapping results from AVIRIS data acquired 19 June 1997 to Hyperion data collected 1 March 2001. Figure 2 shows reference images for the AVIRIS and Hyperion data.

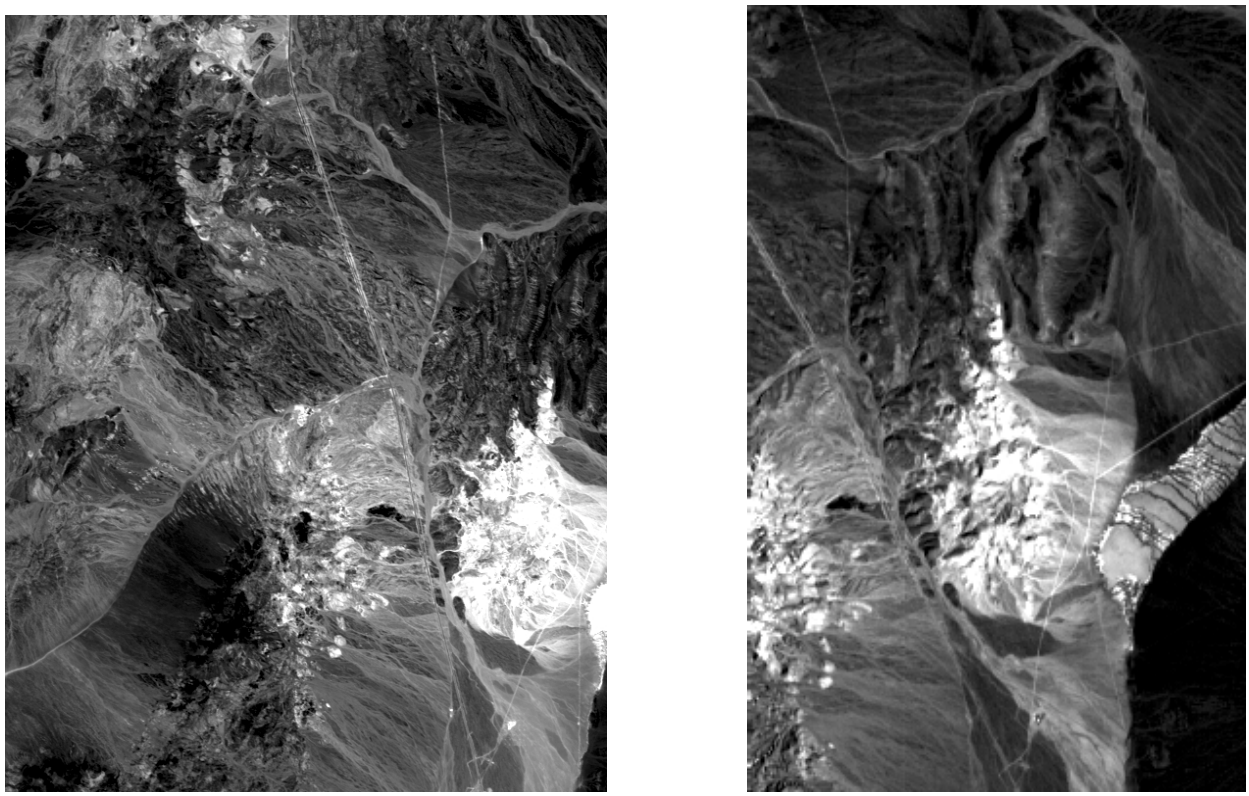

Figure 2: Reference images showing the AVIRIS (left) and Hyperion (right) coverage of the Cuprite, Nevada site. The site is typically described as consisting of two hydrothermal centers (Swayze, 1997). These can be seen in the images as bright areas to the right and left of the road running from NW to SE across the scenes.

3.2 Methods

AIG has developed standardized methods for analysis of hyperspectral data (Figure 3) (Kruse et al., 1996; Kruse and Boardman, 2000). Both the AVIRIS and Hyperion data were processed to geologic products using these AIG-developed approaches for extraction of mineralogic and geologic information. This hyperspectral analysis methodology includes 1) data pre-processing (as required), 2) correction of data to apparent reflectance using the ACORN™ atmospheric correction software, 3) linear transformation of the reflectance data to minimize noise and determine data dimensionality, 4) location of the most spectrally pure pixels, 5) extraction and automated identification of endmember spectra, and 6) spatial mapping and abundance estimates for specific image endmembers. A key point of this methodology is the reduction of data in both the spectral and spatial dimensions to locate, characterize, and identify a few key endmember spectra that can be used to explain the rest of the hyperspectral dataset. Once these endmembers are selected, then their location and abundances can be mapped from the original data. These methods derive the maximum information from the hyperspectral data themselves, minimizing the reliance on *a priori* or outside information.

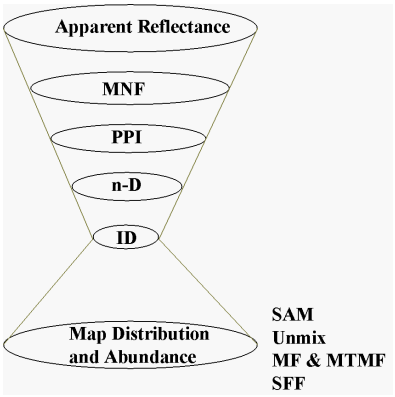

Figure 3: AIG Standardized Processing methods for hyperspectral data analysis.

3.2.1 Destriping for Hyperion area array data

If required, preprocessing/data clean-up may be applied to the data prior to atmospheric correction. In the case of Hyperion data, though radiometric corrections were applied prior to data delivery to AIG, there was still a pronounced vertical striping pattern in the data (visible in individual bands, but more pronounced when using the linearly transformed data). Such striping is apparently caused by dark current imbalances (DC Bias) of the detectors across the pixel direction of the detector (Dykstra and Segal, 1985). This is often seen in data acquired using push-broom (area array) technology (eg: AIS, Hyperion). Destriping was accomplished using custom software (following the model of software written for the original pushbroom imaging spectrometer AIS) (Dykstra and Segal, 1985; Kruse, 1988). This approach adjusts each image column brightness (in all bands) based on a calculated offset relative to the scene average detector response. Assumptions made were that individual detectors were reasonably well behaved (stable) and that over the course of a data collect ("flightline"), that each of the cross-track detectors has covered, on the average, very similar surface materials. Implementation consisted of calculation of an average spectrum for each of the 256 Hyperion detectors followed by determination of a global scene average spectrum. Each column spectrum was then subtracted from the global spectrum to determine offsets to be added to each pixel in the corresponding column. Each pixel in each column of the radiance data was then adjusted accordingly using the calculated offset. Destriping is only required for correcting the pushbroom Hyperion data and thus no destriping was applied to the AVIRIS data.

3.2.2 Atmospheric Correction

The AIG analysis methods are generally applicable to both airborne and satellite data. The methodology requires processing radiance-calibrated data to apparent reflectance. ACORN, currently used by AIG for correction of both airborne and satellite hyperspectral data (AIG, 2001), is a commercially-available, enhanced atmospheric model-based software that uses licensed MODTRAN4 technology to produce high quality surface reflectance without ground measurements. The Cuprite AVIRIS and Hyperion data were both converted to apparent reflectance using ACORN. Appropriate model parameters for each instrument and collection date were used, otherwise, all other parameters were identical for both datasets.

3.2.3 Standardized AIG Hyperspectral Analysis

Standardized AIG hyperspectral analysis methods used for both the airborne sensors and Hyperion data (implemented in the ENVI™ image analysis software) include spectral polishing using "EFFORT" (Boardman, 1998a), spectral data reduction using the Minimum Noise Fraction (MNF) transformation (Green et al, 1988; Boardman, 1993), spatial data reduction using the Pixel Purity Index™ (PPI) (Boardman, 1993), an n-Dimensional Visualizer™ to determine image endmembers (Boardman, 1993), identification of endmembers using their reflectance spectra (Kruse et al, 1993a) in the Spectral Analyst™, and mineral mapping using both the Spectral Angle Mapper (SAM) (Kruse et al., 1993b) and Mixture-Tuned-Matched Filtering (MTMF™) (Boardman, 1998b). This approach is shown in Figure 1 below and also outlined in Kruse et al. (1996) and Kruse and Boardman (2000).

3.2.4 Geometric Corrections

The final step in the analysis is usually to present the results on a map base. In this case, to facilitate comparison of the Hyperion data to AVIRIS mineral mapping results and minimize resampling artifacts, the AVIRIS data were used as the base rather than a map. The Hyperion data were geometrically corrected to match the AVIRIS data by picking ground control points (GCP) and using a 1st degree polynomial warp with nearest neighbor resampling. Approximately 20 GCPs were used and the residual errors were on the order of 2 pixels. Hyperion image-maps (not the full data cube!) were geocorrected to match the AVIRIS data.

3.3 Results

Operationally, spectral bands covering the short wave infrared (SWIR) spectral range (2.0 – 2.5 μm for AVIRIS and 2.0 – 2.4 μm for Hyperion) were selected and these bands were linearly transformed using the MNF transformation. Figure 4 shows a plot of the MNF eigenvalues for both datasets. Higher eigenvalues generally indicate higher information content. The MNF results indicate that the AVIRIS data contain significantly more information than the Hyperion data covering approximately the same spatial area and spectral range. The actual data dimensionality is usually determined by comparing both the eigenvalue plots and the MNF images for each dataset (Figures 4, 5, and 6). In the case of AVIRIS, the MNF analysis indicates a dimensionality of approximately 20. The Hyperion data exhibits dimensionality of approximately 6.

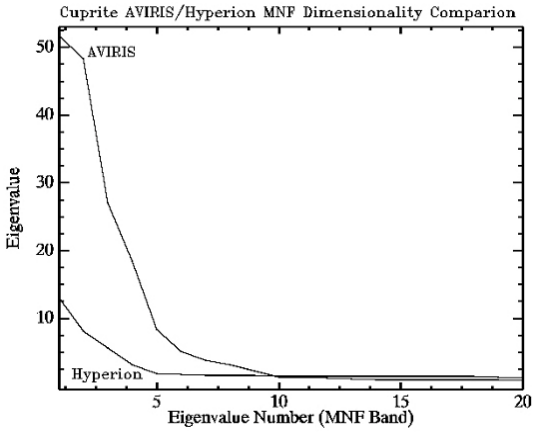

Figure 4: MNF Eigenvalue plots for the Cuprite, Nevada, AVIRIS and Hyperion data

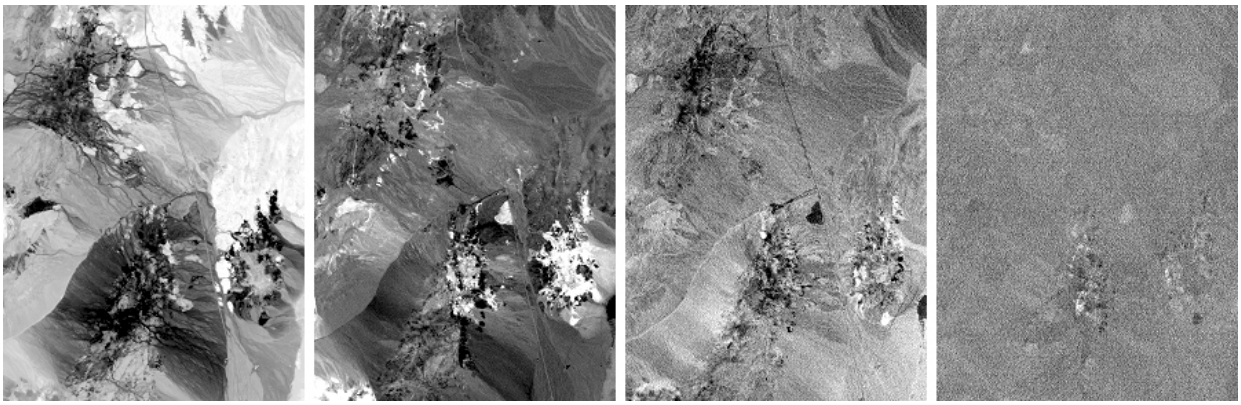

Figure 5. MNF images for the AVIRIS SWIR data. Images from left to right, MNF band 1, MNF band 5, MNF band 10, MNF band 20.

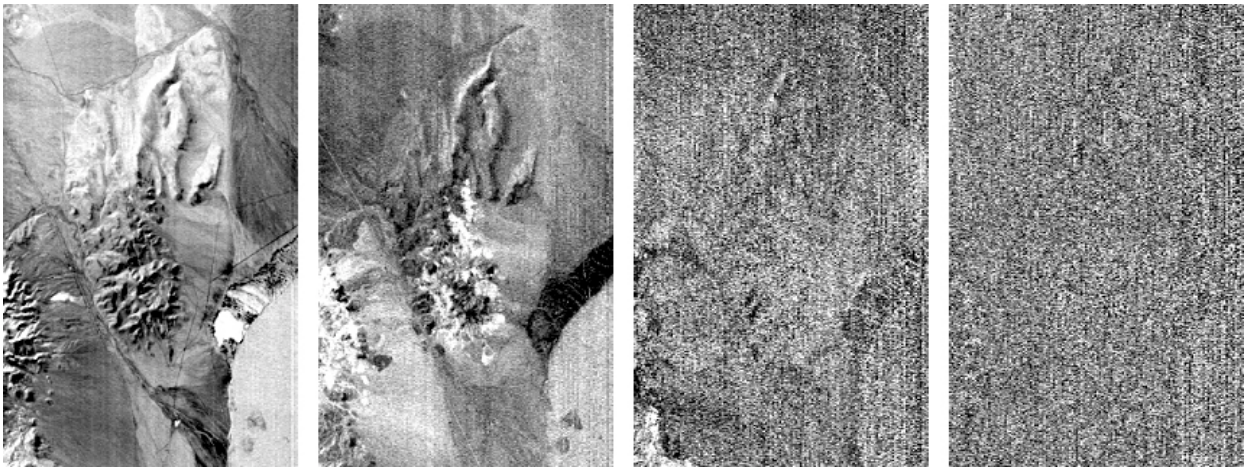

Figure 6. MNF images for the Hyperion SWIR data. Images from left to right, MNF band 1, MNF band 2, MNF band 5, MNF band 10.

The top MNF bands for each data set (20 for AVIRIS, 6 for Hyperion), which contain most of the spectral information (Green et al., 1988), were used to determine the most likely endmembers using the PPI procedure. These potential endmember spectra were loaded into an n-dimensional scatterplot and rotated in real time on the computer screen until "points" or extremities on the scatterplot were exposed (Boardman, 1993). These projections were "painted" using region-of-interest (ROI) definition procedures and then rotated again in 3 or more dimensions (3 or more MNF bands) to determine if their signatures were unique in the MNF data. Once a set of unique pixels were defined, then each separate projection on the scatterplot (corresponding to a pure endmember) was exported to a ROI in the image. Mean spectra were then extracted for each ROI from the apparent reflectance data to act as endmembers for spectral mapping (Figure 7). These endmembers or a subset of these endmembers (in the case of AVIRIS) were used for subsequent classification and other processing. Mixture-Tuned-Matched Filtering (MTMF), a spectral matching method (Boardman, 1998b), was used to produce image-maps showing the distribution and abundance of selected minerals. (Note: MNF endmember spectra, not reflectance spectra are used in the MTMF). The results are generally presented as gray-scale images (not shown) with values from 0 to 1.0, which provide a means of estimating mineral abundance. Brighter pixels in the images represent higher mineral abundances. Results images for both AVIRIS and Hyperion were produced by correcting the Hyperion data to match the AVIRIS spatial scale and orientation as described above. Selected results were combined as color-coded images to show the distribution of the principal (spectrally predominant) minerals (Figure 8).

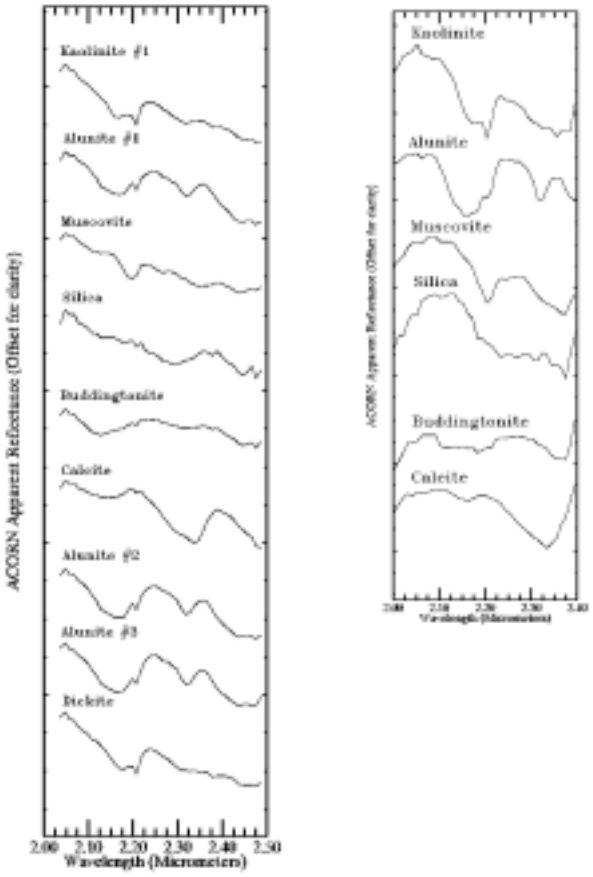

Figure 7: Comparison of selected AVIRIS endmember spectra (left) and Hyperion endmember spectra (right). Note that AVIRIS detected several varieties of alunite plus an additional kaolinite-group mineral (dickite) that were not detectable using the Hyperion data. Other AVIRIS minerals and vegetation not shown.

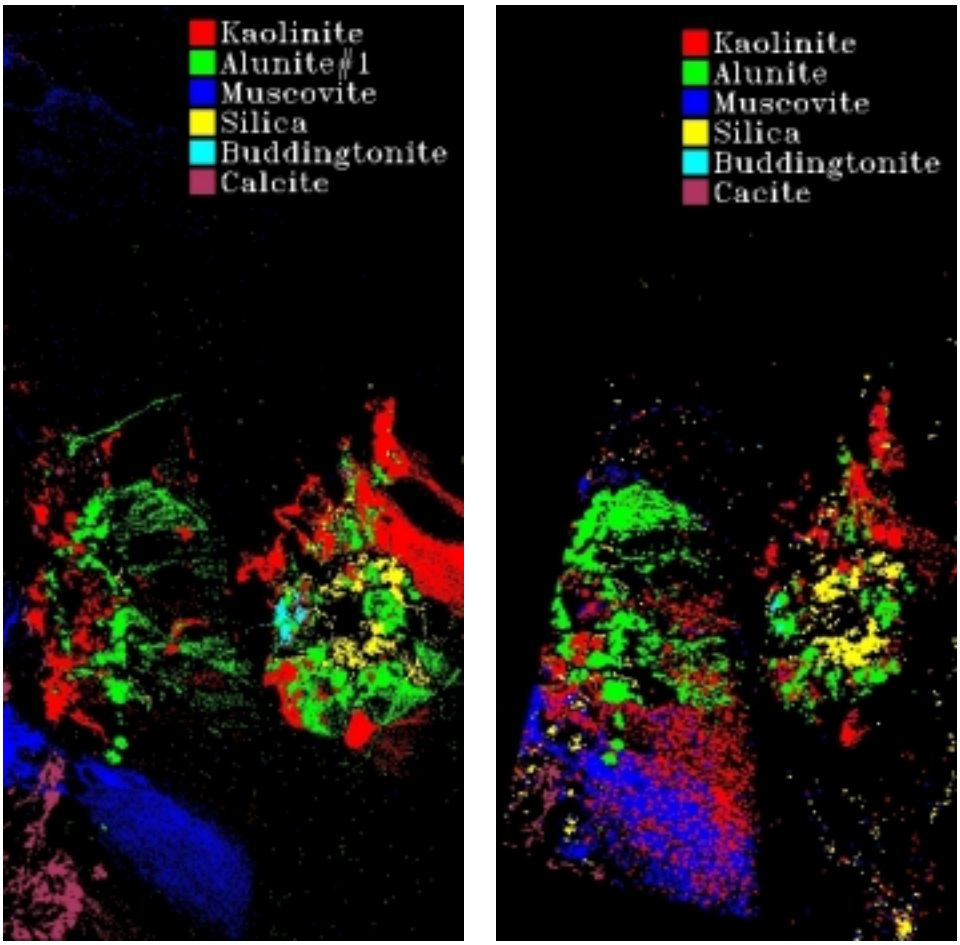

Figure 8: MTMF mineral maps for AVIRIS (left) and Hyperion (right) produced using the endmember spectra in Figure 7.

Visual comparison of the two classified datasets shows that Hyperion identifies similar minerals and produces similar mineral mapping results to AVIRIS. In this case, the difference in pixel size is generally inconsequential (causing only slight loss of spatial detail in Hyperion results). It seems likely that the lower SNR of the Hyperion data (specified at approximately 50:1 vs >500:1 for AVIRIS) does affect the ability to extract characteristic spectra and identify individual minerals. (See the Hyperion buddingtonite spectrum in Figure 7 above, which does not clearly show the characteristic buddingtonite spectral feature shape near 2.11 μm, which is well resolved in AVIRIS [Figure 7] and other hyperspectral aircraft data) (Kruse et al., 1990, 2000; Swayze, 1997; Green et al., 2001). This spectrum could also, however, be an effect of the pixel size causing greater mixing in the Hyperion data for relatively small buddingtonite occurrences. Additionally, bear in mind that Figure 8 shows a basic AVIRIS mineral map. It is possible to extract more detailed mineralogic information from the AVIRIS data (Swayze, 1997; Green et al., 2001; Kruse et al., 2001, 2002;) as well as abundance information (Boardman and Kruse, 1994; Boardman et al., 1995, Kruse et al, 1999). Determination of abundances for minerals identified by Hyperion is possible, but not illustrated here. Our analysis also indicates that the Cuprite Hyperion data do not allow extraction of the same level of detailed mineralogic information as AVIRIS (eg: within-species separation of micas and temperature mapping of Alunites) (Swayze, 1997; Swayze et al., 1992). Actually though, Hyperion performs surprisingly well considering the overall SWIR SNR.

3.4 Accuracy Assessment and Error Analysis

Visual comparison of the Hyperion and AVIRIS MTMF image maps in Figure 8 using the AVIRIS data as the "Ground Truth" indicates that in general, using these mapping methods, the two datasets produce similar mapping results. Figure 9 shows a comparison of MTMF results for the minerals kaolinite and alunite, presented as binary

images covering the data's overlapping area (white is a specific mineral, black is unclassified), and it can be seen that these have similar patterns of classified pixels for the selected minerals.

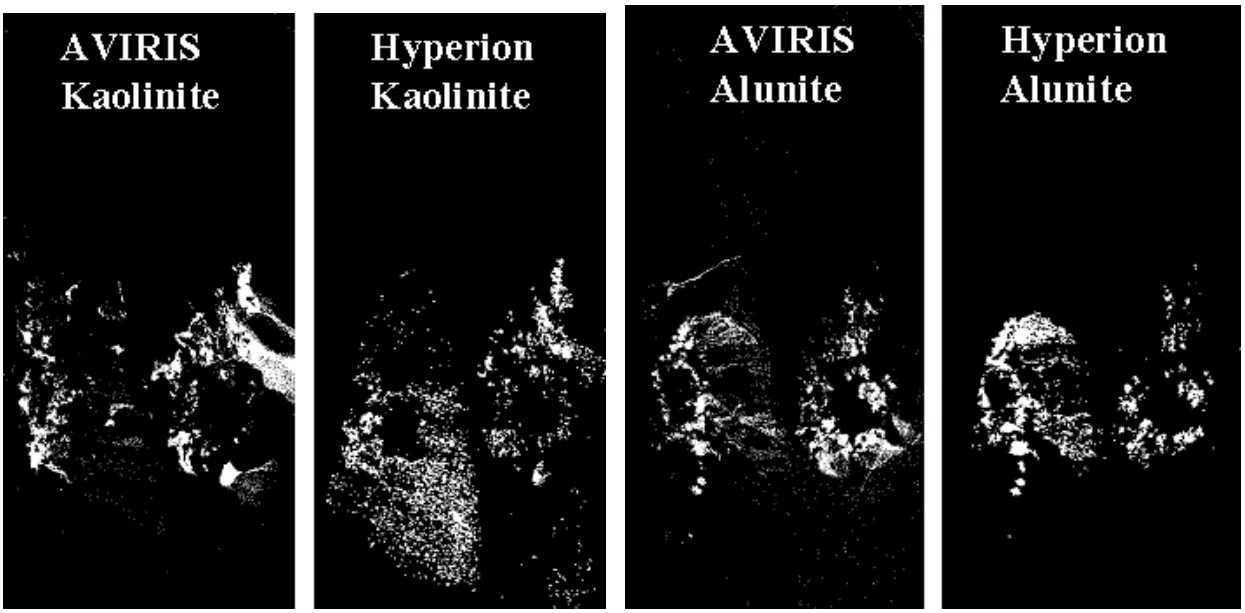

Figure 9: Comparison of MTMF mineral mapping results for kaolinite and alunite. White pixels indicate successful classification.

Detailed direct comparison of the mapping results demonstrates, however, that the correspondence is not as great as may be thought from visual comparison. Comparison of the MTMF spectral mapping results using a confusion matrix approach shows that many pixels classified using AVIRIS are unclassified on Hyperion (up to 60%, but variable by mineral). These are errors of omission. This is probably explained by the differences in SNR between the two datasets. Some spectral features are simply below the level of detection on the Hyperion data (This issue is explored further in a later section). The same analysis, but excluding the unclassified areas, yields approximately 75% overall agreement of Hyperion to AVIRIS, with a Kappa Coefficient of 0.66 (Table 2) (Richards, 1994). This highlights errors of commission (where pixels mapped as one mineral by AVIRIS are mapped as another mineral by Hyperion). First, some pixels unclassified using AVIRIS are misclassified as a specific mineral on Hyperion (around 5% commission error). Additionally, some pixels classified by AVIRIS as specific minerals are misclassified as different minerals on Hyperion (~25% commission error). Specifically, there is minor classification error between: Kaolinite mapped by Hyperion as Muscovite (7%), Kaolinite and Silica (4%), Muscovite and Calcite (2%), Silica and Alunite (6%), Silica and Muscovite (3%), Silica and Calcite (1%), Buddingtonite and Kaolinite (7%), Calcite and Muscovite (5%), and Calcite and Silica (4%). Moderate errors occur between:, Kaolinite mapped by Hyperion as Alunite (15%), Alunite and Kaolinite (16%), and Silica and Kaolinite (13%). The highest errors occur between: Buddingtonite mapped by Hyperion as Alunite (58%), and Muscovite mapped by Hyperion as Kaolinite (25%). Table 2 summarizes the error relationships between minerals.

Table 2: Confusion Matrix comparing Hyperion MTMF mapping results to AVIRIS "Ground Truth" MTMF results.

	AVIRIS "Ground Truth" Class (Percent)						
Hyperion	Kaolinite %	Muscovite %	Silica %	Buddingtonite %	Alunite%	Calcite %	Total %
Kaolinite	73.13	25.09	12.87	7.02	16.39	2.66	36.20
Muscovite	7.14	72.58	2.52	0.00	0.88	4.56	20.63
Silica	4.33	0.79	76.96	0.00	2.23	4.18	8.70
Buddingtonite	0.02	0.00	0.00	35.09	0.49	0.00	0.61
Alunite	14.83	0.00	6.39	57.89	79.68	0.00	31.38
Calcite	0.55	1.54	1.26	0.00	0.33	88.59	2.48
Total	100.00	100.00	100.00	100.00	100.00	100.00	100.00

While this comparison serves to highlight the accuracy and overall performance of the Hyperion dataset compared to AVIRIS, several other issues may affect the accuracy assessment. These include: 1) the data coverage (spatial extent) of the two datasets – they cover substantially the same ground, but not exactly (affects unclassified class), 2) the data pixel size (AVIRIS is 20m, Hyperion 30m), 3) Image acquisition differences (date/time, atmospheric conditions, SNR), 4) slightly different spectral characteristics (2.0 – 2.5 μm for AVIRIS vs 2.0 – 2.4 μm for Hyperion; varying band centers and spectral resolution), 5) different image-based endmembers spectra used for MTMF (endmember spectra not identical), 6) MTMF threshold consistency and class combining (AVIRIS), and 7) Hyperion to AVIRIS image registration accuracy.

4.0 SNR COMPARISONS – EFFECT ON MINERAL MAPPING

Previous Hyperion investigations show that there is a strong relationship between the acquisition time of year and the signal-to-noise ratio (SNR) of the Hyperion data (Kruse et al., 2001, 2002). SNR for the same targets are higher in the summer and lowest in the winter. This has a direct effect on spectral mineral mapping, with lower SNR resulting in extraction of less detail (also see AVIRIS vs Hyperion MNF comparison above). Calculation of data SNR using a Mean/Standard Deviation method for a homogeneous target (Stonewall Playa) produces the results shown in Figure 10 for the Cuprite AVIRIS (June 1997) and Hyperion (March 2001). While these SNR are representative of those that can be extracted directly from the data, slightly higher SNR could probably be obtained through analysis of the data dark current signal. Figure 10 also shows calculated SNR for Hyperion data collected during July 2001 (northern hemisphere summer) for a site in northern Death Valley, California. All SNR are normalized to 50% reflectance. Note that the SWIR SNR is significantly higher than the calculated Cuprite SWIR SNR for the March 2001 data (SWIR SNR ~50:1 vs 25:1). The implications of the decreased Hyperion winter SNR are evident in endmember spectra extracted from both the Cuprite AVIRIS and Hyperion (Figure 7) and the northern Death Valley Hyperion data (Figure 11).

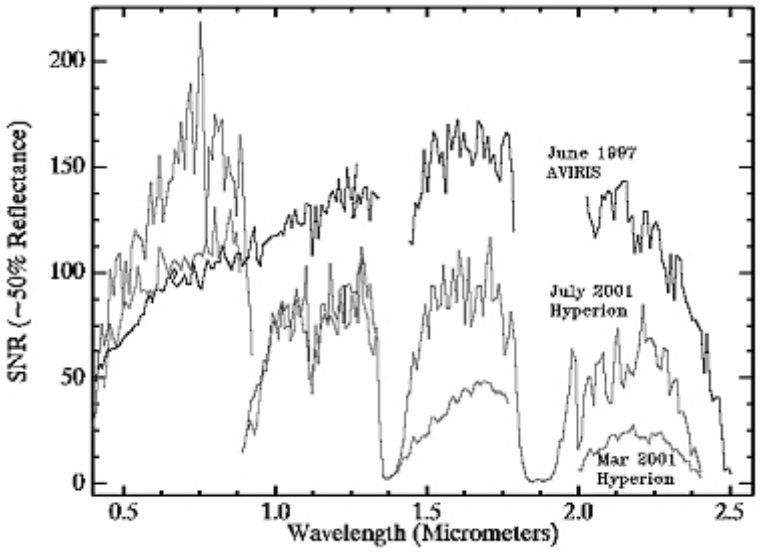

Figure 10: SNR Comparisons for June 1997 AVIRIS, July 2001 Hyperion, and March 2001 Hyperion.

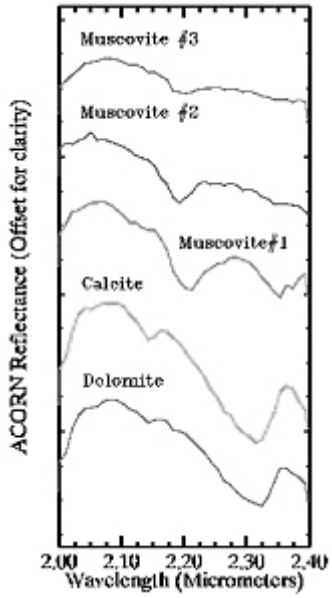

Figure 11: Northern Death Valley Hyperion Spectral Endmembers

While the Cuprite Hyperion data allow basic mineral identification, more detail (additional endmembers) are detected and mapped using the higher SNR AVIRIS and Hyperion data. This is also important for geologic/mineral mapping, because higher SNR allows separation of similar endmembers such as calcite from dolomite (Figure 11) and within-species variability such as kaolinite vs dickite (Figure 7). In the northern Death Valley case, the high SNR allows detection of 3 different mica endmembers with different aluminum substitution (Kruse et al., 1999). Previous investigations have indicated that SNR is critical for this determination (Kruse et al., 1999, 2001, 2002).

5.0 Conclusions

Analysis of Hyperion data for Cuprite, Nevada, which has established ground truth and years of airborne hyperspectral data, show that Hyperion is performing to specifications and data from the short wave infrared (SWIR) spectrometer can be used to produce useful geologic (mineralogic) information. Airborne Visible/Infrared Imaging Spectrometer (AVIRIS) data collected during June 1997 served as the "ground truth" for this investigation. Comparison of Hyperion results to the known mineralogy derived from AVIRIS data generally validate on-orbit mineral mapping and Hyperion performance. Minerals mapped at Cuprite using Hyperion include kaolinite, alunite, buddingtonite, calcite, muscovite, and hydrothermal silica. This case history demonstrates the analysis methodologies and level of information available from these Hyperion data. It also demonstrates the importance of high signal-to-noise performance for hyperspectral sensors. The Cuprite Hyperion data represent an "early" Hyperion acquisition for the northern hemisphere (a winter scene); thus the SWIR signal-to-noise ratio (SNR) (Mean/Standard Deviation method on Stonewall Playa) is approximately 25:1. Other Hyperion scenes collected under optimum (summer) conditions exhibit SWIR SNR as high as approximately 50:1. The level of mineralogic information available from the data is directly tied to the SNR.

Standardized hyperspectral data processing methods applied to the Cuprite Hyperion data lead to definition of specific key minerals, however, it is more difficult (than for AVIRIS) to extract the information because of the Hyperion data's lower SNR. The effect of this reduced response compared to AVIRIS is lower data dimensionality, thus fewer endmembers can be identified and mapped than with AVIRIS. Accuracy assessment and error analysis indicates that with these Cuprite Hyperion data that, in many cases, mineral identification is not possible where specific minerals are known to exist. Detailed direct comparison of mixture-tuned-matched-filtering (MTMF) spectral mapping results using a confusion matrix approach shows that many pixels classified using AVIRIS are unclassified on Hyperion (up to 60%, but variable by mineral). These are errors of omission. This is probably explained by the differences in SNR between the two datasets. Some spectral features are simply below the level of detection on the Hyperion data. The same analysis, but excluding the unclassified areas, yields approximately 75% overall agreement of Hyperion to AVIRIS, with a Kappa Coefficient =0.66. This highlights errors of commission (where pixels mapped as one mineral by AVIRIS are mapped as another mineral by Hyperion). First, some pixels unclassified using AVIRIS are misclassified as a specific mineral on Hyperion (around 5% commission error). Additionally, some pixels classified by AVIRIS as specific minerals are misclassified as different minerals on Hyperion (~25% commission error). The highest errors occur between: Buddingtonite mapped by Hyperion as Alunite (58%), and Muscovite mapped by Hyperion as Kaolinite (25%).

As a technology demonstration, Hyperion performs surprisingly well for mineral identification and mapping. We expect (and have demonstrated) improved mineral identification and mapping results from "summer" season Hyperion acquisitions with higher SNR than the Cuprite data. These improvements principally take the form of mapping of subtle distinctions such as determining the difference between calcite and dolomite and mapping within-species variability caused by molecular substitution (eg: aluminum substitution in micas). Unfortunately, Hyperion data collected under less than optimum conditions (winter season, dark targets) have marginal SWIR SNR and allow mapping of only the most basic mineral occurrences and mineral differences (Kruse et al., 2001, 2002). This results in a recommendation that future HSI satellite sensors have significantly higher SNR performance specifications than Hyperion for the SWIR (at least 100:1 based on dark current measurements).

6.0 Acknowledgements

This research was partially funded by NASA under grant NCC5-495. Additional financial support was provided by Analytical Imaging and Geophysics LLC internal research and development funds. AVIRIS data were provided by JPL. ACORN is a trademark of ImSpec Associates, LLC. ENVI is a registered trademark of Research Systems Inc., Boulder, Colorado. Pixel Purity Index (PPI), n-Dimensional Visualizer, Spectral Analyst, and Mixture-Tuned Matched Filter (MTMF) are all trademarks of Research Systems Inc.

7.0 References

Abrams, M. J., Ashley, R. P., Rowan, L. C., Goetz, A. F. H., and Kahle, A. B., 1977, Mapping of hydrothermal alteration in the Cuprite mining district, Nevada, using aircraft scanner images for the spectral region 0.46 – 2.36 μm, *Geology*, v. 5, p. 713-718.

AIG, 2001, *ACORN User's Guide, Stand Alone Version: Analytical Imaging and Geophysics LLC*, 64 p.

Ashley, R. P., and Abrams, M. J., 1980, Alteration mapping using multispectral images-Cuprite Mining District, Esmeralda County, Nevada: *U.S. Geological Survey Open File Report 80-367*, 17 p.

Boardman, J. W., 1993, Automated spectral unmixing of AVIRIS data using convex geometry concepts: in *Summaries, Fourth JPL Airborne Geoscience Workshop, JPL Publication 93-26*, v. 1, p. 11-14

Boardman J. W., and Kruse, F. A., 1994, Automated spectral analysis: A geologic example using AVIRIS data, north Grapevine Mountains, Nevada: in *Proceedings, Tenth Thematic Conference on Geologic Remote Sensing*, Environmental Research Institute of Michigan, Ann Arbor, MI, p. I-407 - I-418.

Boardman, J. W., Kruse, F. A., and Green, R. O., 1995, Mapping target signatures via partial unmixing of AVIRIS data: in *Summaries, Fifth JPL Airborne Earth Science Workshop, JPL Publication 95-1*, v. 1, p. 23-26.

Boardman, J. W., 1998a, Post-ATREM polishing of AVIRIS apparent reflectance data using EFFORT: a lesson in accuracy versus precision, in *Summaries of the Seventh JPL Airborne Earth Science Workshop*, v. 1, p. 53.

Boardman, J. W., 1998b, Leveraging the high dimensionality of AVIRIS data for improved sub-pixel target unmixing and rejection of false positives: mixture tuned matched filtering, in: *Summaries of the Seventh Annual JPL Airborne Geoscience Workshop*, Pasadena, CA, p. 55.

Clark, R. N., King, T. V. V., Klejwa, M., and Swayze, G. A., 1990, High spectral resolution spectroscopy of minerals: *Journal of Geophysical Research*, v. 95, no. B8, p. 12653-12680.

Dykstra, J. D., and Segal, D. B., 1985, Analysis of AIS data of the Recluse Oil Field, Recluse, Wyoming: *in Proceedings, AIS workshop, 8-10 April, 1985, JPL Publication 85-41*, Jet Propulsion Laboratory, Pasadena, California, p. 86-91.

Goetz, A. F. H., and Strivastava, V., 1985, Mineralogical mapping in the Cuprite Mining District: In *Proceedings of the Airborne Imaging Spectrometer (AIS) Data Analysis Workshop, JPL Publication 85-41*, p. 22-29.

Goetz, A. F. H., G. Vane, J. E. Solomon, and B. N. Rock, 1985. Imaging spectrometry for earth remote sensing, *Science*, v. 228, p. 1147 - 1153.

Goetz, A. F. H., and Kindel, B., 1996, Understanding unmixed AVIRIS images in Cuprite, NV using coincident HYDICE data: in *Proceedings, 6th JPL Airborne Earth Science Workshop: Jet Propulsion Laboratory Publication 96-4*, v. 1.

Green, A. A., Berman, M., Switzer, B., and Craig, M. D., 1988, A transformation for ordering multispectral data in terms of image quality with implications for noise removal: *IEEE Transactions on Geoscience and Remote Sensing*, v. 26, no. 1, p. 65 - 74.

Green, R.O., B.J. Chippendale, C. Chovit, T. Chrien, S. Dilanchian,, M. Eastwood, J. Faust, V. Grigoryan, J. Holbrook, F. Loaiza, S. Lundeen, I. McCubbing, B. Pavri, J. Raney, C. Sarture, M. Solis, 2001, Overview of the AVIRIS 2000 Flight Season: in *Proceedings of the 10th JPL Airborne Earth Science Workshop: Jet Propulsion Laboratory Publication*, (in press).

Hook, S. J., 1990; The combined use of multispectral remotely sensed data from the short wave infrared (SWIR) and thermal infrared (TIR) for lithological mapping and mineral exploration: in *Proceedings, Fifth Australasian Remote Sensing Conference, Perth, Western Australia*, v. 1, p. 371 – 380.

Kruse, F. A., 1988, Use of Airborne Imaging Spectrometer data to map minerals associated with hydrothermally altered rocks in the northern Grapevine Mountains, Nevada and California: *Remote Sensing of Environment*, v. 24, no. 1, pp. 31-51.

Kruse, F. A., Kierein-Young, K. S., and Boardman, J. W., 1990, Mineral mapping at Cuprite, Nevada with a 63 channel imaging spectrometer: *Photogrammetric Engineering and Remote Sensing*, v. 56, no. 1, p. 83-92.

Kruse, F. A., and Lefkoff, A. B., 1993, Knowledge-based geologic mapping with imaging spectrometers: *Remote Sensing Reviews*, Special Issue on NASA Innovative Research Program (IRP) results, v. 8, p. 3 - 28.

Kruse, F. A., Lefkoff, A. B., and Dietz, J. B., 1993a, Expert System-Based Mineral Mapping in northern Death Valley, California/Nevada using the Airborne Visible/Infrared Imaging Spectrometer (AVIRIS): *Remote Sensing of Environment, Special issue on AVIRIS, May-June 1993*, v. 44, p. 309 - 336.

Kruse, F. A., Lefkoff, A. B., Boardman, J. B., Heidebrecht, K. B., Shapiro, A. T., Barloon, P. J., and Goetz, A. F. H., 1993b, The Spectral Image Processing System (SIPS) - Interactive Visualization and Analysis of Imaging Spectrometer Data: *Remote Sensing of Environment, Special issue on AVIRIS, May-June 1993*, v. 44, p. 145 - 163.

Kruse, F. A., Huntington, J. H., and Green, R. O, 1996, Results from the 1995 AVIRIS Geology Group Shoot: in *Proceedings, 2nd International Airborne Remote Sensing Conference and Exhibition*: Environmental Research Institute of Michigan (ERIM), Ann Arbor, v. I, p. I-211 - I-220.

Kruse, F. A., Boardman, J. W., and Huntington, J. F., 1999, Fifteen Years of Hyperspectral Data: northern Grapevine Mountains, Nevada: in Proceedings of the 8th JPL Airborne Earth Science Workshop: Jet Propulsion Laboratory Publication, *JPL Publication 99-17*, p. 247 - 258.

Kruse, F. A., and Boardman, J. W., 2000, Characterization and Mapping of Kimberlites and Related Diatremes Using Hyperspectral Remote Sensing: in Proceedings, 2000 IEEE AeroSpace Conference, 18 – 24 March 2000, Big Sky, Montana.

Kruse, F. A., Boardman, J. W., Lefkoff, A. B., Young, J. M., Kierein-Young, K. S., Cocks, T. D., Jenssen, R., and Cocks, P. A., 2000, The AIG/HyVista 1999 USA HyMap Group Shoot: Overview and Analysis Examples: in *Proceedings IGARSS 2000, 24 – 28 July, 2000, Honolulu, Hawaii*, IEEE, Catalog Number 00CH37120C, ISBN 0-7803-6362-0, published on CD-ROM.

Kruse, F. A., Boardman, J. W., and Huntington, J. F., 2001, Progress Report: Geologic Validation of EO-1 Hyperion: in *Proceedings of the 10th JPL Airborne Earth Science Workshop: Jet Propulsion Laboratory Publication*. (in-press).

Kruse, F. A., Boardman, J. W., and Huntington, J. F., 2002, Comparison of EO-1 Hyperion and Airborne Hyperspectral Remote Sensing Data for Geologic Applications: in *Proceedings, SPIE Aerospace Conference, 9-16 March 2002, Big Sky, Montana* (in press).

Pearlman, J, Stephen Carman, Paul Lee, Lushalan Liao and Carol Segal, 1999, Hyperion Imaging Spectrometer on the New Millennium Program Earth Orbiter-1 System: In *Proceedings, International Symposium on Spectral Sensing Research (ISSSR), Systems and Sensors for the New Millennium, published on CD-ROM, International Society for Photogrammetry and Remote Sensing (ISPRS).*

Porter, W. M., and Enmark, H. E., 1987, System overview of the Airborne Visible/Infrared Imaging Spectrometer (AVIRIS), in *Proceedings, Society of Photo-Optical Instrumentation Engineers (SPIE)*, v. 834, p. 22-31.

Richards, J.A., 1994, *Remote Sensing Digital Image Analysis, An Introduction*, Springer-Verlag, New York, pp. 271 – 275.

Shipman, H. and Adams, J. B., 1987, Detectability of minerals on desert alluvial fans using reflectance spectra, *Journal of Geophysical Research*, v. 92, no. B10, p. 10391-10402.

Swayze, G. A., 1997, The hydrothermal and structural history of the Cuprite Mining District, southwestern Nevada: An integrated geological and geophysical approach: *Unpublished Ph. D. thesis, University of Colorado, Boulder*, 341 p.

Swayze, G. A., Clark, R. L., Sutley, S. and Gallagher, A. J., 1992, Ground-truthing AVIRIS mineral mapping at Cuprite, Nevada: in *Summaries of the Third Annual JPL Airborne Geosciences Workshop, V 1., AVIRIS Workshop, JPL Publication 92-14*, p. 47 – 49.